ACS APPLIED MATERIALS & INTERFACES

Research Article

www.acsami.org

Conjugated Polymer Chain and Crystallite Orientation Induced by Vertically Aligned Carbon Nanotube Arrays

Seok-Ju Kang,[†,¶] Youn-Su Kim,[¶] Won Bae Kim,[¶] Dong-Yu Kim,*[,¶] and Yong-Young Noh*[,†]

[†]Department of Energy and Materials Engineering, Dongguk University, 26 Pil-dong, 3 ga, Jung-gu, Seoul 100-715, Republic of Korea

[¶]School of Material Science and Engineering, Gwangju Institute of Science and Technology (GIST), 261 Cheomdangwagiro (Oryong-dong), Buk-gu, Gwangju 500-712, Republic of Korea

Supporting Information

ABSTRACT: We report a method for controlling the orientations of conjugated polymers in the active layer of organic thin-film transistors (OTFTs) by annealing the film at the melting temperature in a vertically aligned multiwalled carbon nanotube (VA-CNT) template under various load pressures. Poly(3-hexylthiophene) [P3HT] molecules are effectively aligned in the melting state annealing at 240 °C for 30 min, as a result of intermolecular $\pi-\pi$ and $CH_3-\pi$ interactions between the polymer and the VA-CNTs, which are separated from the conjugated polymer film after cooling to room temperature. In-plane and out-of-plane X-ray diffraction results show that the melt-annealed P3HT film with VA-CNTs has better crystallite ordering than a pristine 80 °C baked film and a melt-annealed film without VA-CNTs, and a larger number of crystallites in the treated P3HT film are oriented in the [100] direction, which is normal to the substrate. When we used the melt-aligned P3HT film with VA-CNTs as the active layer in OTFTs, the P3HT OTFT exhibits a better field-effect mobility value of 0.12 $cm^2/(V\ s)$ than a simply melt-annealed device without VA-CNTs [0.06 $cm^2/(V\ s)$].

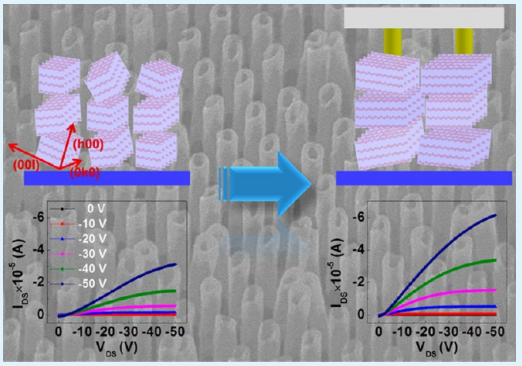

KEYWORDS: *conjugated polymer, orientation of crystallite, organic thin film transistors, carbon nanotube, crystallinity of polymer, charge carrier mobility*

INTRODUCTION

Control of the packing and orientation of conjugated molecules in the bulk state or at the semiconductor/dielectric layer interface is highly important for improving the performances of various organic electronic devices, such as organic thin-film transistors (OTFTs),[1−6] organic light-emitting diodes,[7,8] and organic photovoltaic devices.[9] For example, the charge carrier mobility is strongly dependent on the molecular crystallinity and orientation in the semiconducting polymer bulk film and at the semiconductor/dielectric interface.[1,5,10] To achieve high mobility in polymer thin-film transistors (TFTs), various approaches have been reported for obtaining better molecular crystallinity and orientation for lateral charge transport through the transistor channel.[11−19] One of the methods commonly used is to modify the surface energy of a dielectric layer or substrate by forming a self-assembled monolayer (SAM), which leads to better molecular orientation at the semiconductor/dielectric interface.[1,5,12,13] The surface energy of a silicon dioxide dielectric layer or a glass substrate is effectively reduced by the formation of an octadecyltrichlorosilane (OTS) or hexamethyldisilazane (HMDS) SAM. The lower surface energy on the dielectric layer enables favorable edge-on orientation of conjugated polymers for lateral charge carrier transport by interactions between the alkyl side chains of conjugated polymers and the terminal methyl groups in SAM molecules.[1,5,13] However, there are certain limitations to obtaining reliable TFT results using the SAM modification method, because of difficulties in fabricating reproducible, smooth, and uniform monolayers to modify the chemical and/or physical properties of SiO_2 surfaces so that silanes could easily polymerize and form rough multilayer in the presence of water.[20] Moreover, typical polymer solutions tend to have dewetting behaviors on hydrophobic surfaces during spin-casting processes. As a result, on SAM (OTS or HMDS)-treated substrates, a wide range of field-effect mobility (μ_{FET}) values [1×10^{-3} to 0.1 $cm^2/(V\ s)$] have been reported from different laboratories for regioregular poly(3-hexylthiophene) [rr-P3HT] OTFTs.[1,14−19,21]

It is thought that conjugated polymer molecules generally intimately wrap carbon nanotubes (CNTs) in the solution state through $CH-\pi$ (between the pendant hexyl group and graphitic walls) and $\pi-\pi$ (between the thiophene ring and the benzene ring of multiwalled carbon nanotubes (MWCNTs)) noncovalent interactions.[22−24] For example, P3HT molecules exhibited an intermixed structure with MWCNTs via noncovalent interactions.[25−27] However, it is difficult to use these interactions to improve the charge carrier mobility in OTFTs by controlling the orientation or packing of

Received: June 10, 2013
Accepted: August 15, 2013
Published: August 15, 2013

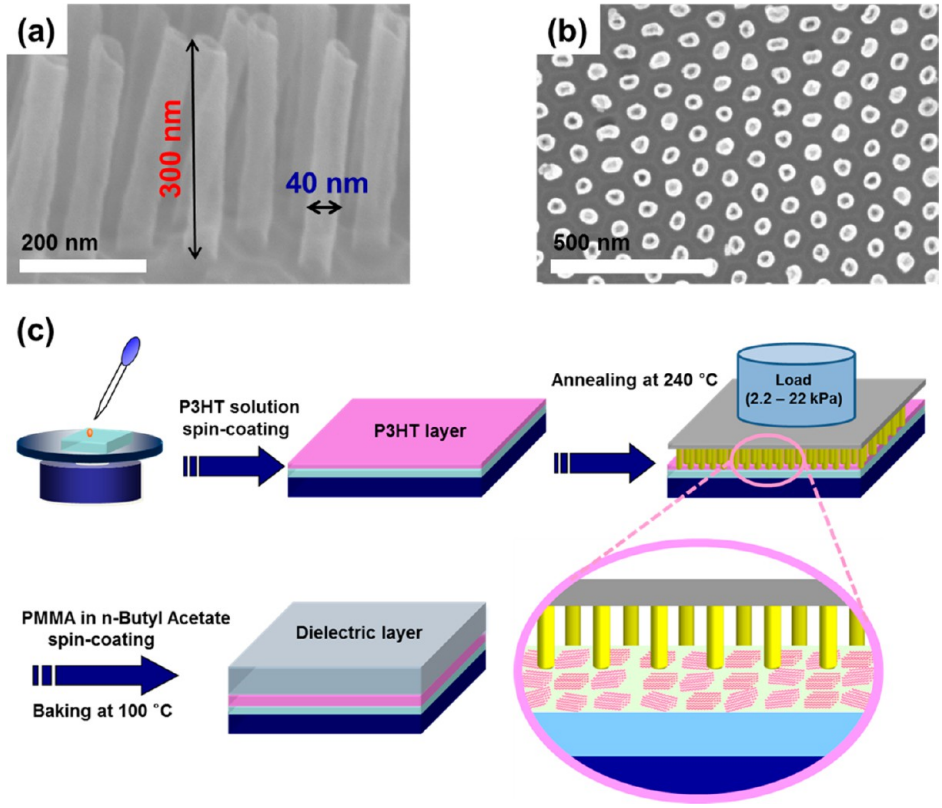

Figure 1. Scanning electron microscopy (SEM) images of VA-CNT array/AAO used for pressed melt-annealing process from (a) cross-sectional and (b) normal view. The CNTs have diameters of ~40 nm and lengths of ~300 nm. (c) Schematic procedure of VA-CNT-array-pressed melt-annealing of P3HT for top-gate and bottom-contact TFTs.

the conjugated molecules, since intermixed metallic and semiconducting CNTs in an active layer of a transistor can distort the OTFT characteristics. Ideally, to improve the orientation of conjugated polymers, uniaxially aligned CNT arrays must be placed proximately with conjugated molecules in a fluidic state, such as in solution, and removed from the active layer of the OTFT after forming a solid film. Uniform nanostructure imprinting and nanotube blending are difficult to achieve, and, to the best of our knowledge, there have only been a few reports on the application of interactions between nanotubes (or holes) and conjugated polymers to obtain better orientation and crystallinity of conjugated molecules for the improved performances of organic electronics.[28−31]

Here, we report a method for controlling the orientations of conjugated polymers in the active layers of OTFTs by annealing the film above the melting temperature in a vertically aligned MWCNT (VA-CNT) template with various load pressures (see Figure 1c). P3HT molecules are effectively aligned in the melt state during annealing at 240 °C for 30 min by intermolecular $\pi-\pi$ and $CH_3-\pi$ interactions between the conjugated polymer and VA-CNTs, which are separated from the polymer film after cooling to room temperature. In-plane and out-of-plane X-ray diffraction (XRD) results show that melt-annealed P3HT films with VA-CNTs have better crystallinities than pristine 80 °C annealed films and solely melt-annealed films without VA-CNT templates, and a larger number of crystallites in the P3HT film are oriented in the [100] direction, which is the direction normal to the substrate. We used melt-aligned P3HT films with VA-CNTs as the active layers of OTFTs. The P3HT OTFT has a field-effect mobility value of 0.12 $cm^2/(V\ s)$, which is nearly twice that of a solely melt-annealed device without VA-CNTs (0.06 $cm^2/(V\ s)$).

EXPERIMENTAL SECTION

Substrate Preparation. A Corning Eagle 2000 glass as the device substrate and a prime-grade silicon wafer (highly n++ doped silicon) with a 300 nm layer of thermally grown oxide were cleaned in an ultrasonic bath with deionized water, acetone, and isopropyl alcohol, sequentially, for 10 min each. The source and drain electrodes were patterned using standard photolithographic methods and were deposited on the cleaned glass by thermal evaporation (Ni/Au = 5/20 nm). The channel lengths were 5, 10, and 20 μm, and the width was 1 mm. Before polymer deposition, the substrates were treated with UV/ozone irradiation for 20 min to clean the surface of the patterned electrode.

Characterization of Films. The formation and structure of the VA-CNT templates, of which fabrication procedure was demonstrated in previous reports,[32,33] were confirmed using scanning electron microscopy (SEM) (Hitachi, Model S-4700) in both normal and cross-sectional views. To investigate thermal properties (such as glass and melting temperature) of the polymer semiconductor (rr-P3HT, Sigma−Aldrich), differential scanning calorimetry (DSC) was carried out using a TA Instruments 2010 series at a heating rate of 10 °C/min under a N_2 atmosphere. Atomic force microscopy (AFM) measurements were performed using a Veeco Digital Instruments Multimode atomic force microscope controlled by a Nanoscope IIIa scanning probe microscope controller in tapping mode with a silicon cantilever, to characterize the surface morphologies of the samples. To determine the light absorption of the P3HT layer under various conditions, ultraviolet−visible−near-infrared (UV-vis_NIR) absorption spectroscopy was performed using a Perkin−Elmer Mode Lambda 12 spectrometer with 1-nm increments. Out-of plane X-ray diffraction (XRD) was performed at room temperature with a Rigaku Model RINT 2000 diffractometer using Cu Kα ($\lambda \approx 1.5418$ Å) radiation.

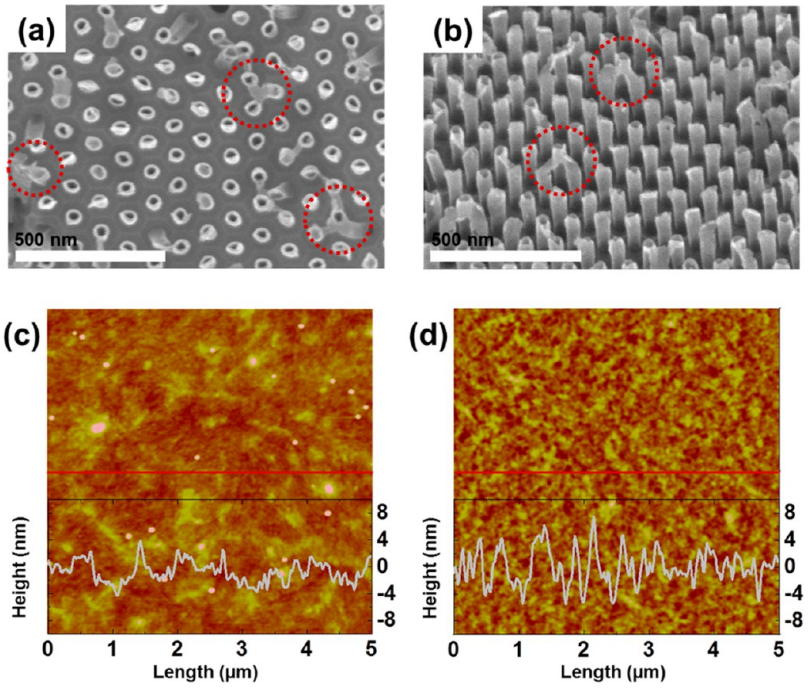

Figure 2. SEM images of VA-CNT arrays after pressing in a melt-annealing process in (a) normal and (b) 45° inclined view. AFM topographical height images (5 μm × 5 μm) of melt-annealed P3HT thin films (c) without and (d) with VA-CNT-array pressing (under 6.5 kPa). Topographical profiles of outlined red sections are indicated at the bottom of the images.

Grazing-incidence XRD (GIXD) measurements were performed at the 10C1 XRS II beamline ($\lambda \approx 1.07$ Å), with an incident energy of 11.56 keV, at the Pohang Accelerator Laboratory (PAL). The X-ray incident angle was fixed at 0.2°, to maximize the diffracted signal and minimize the background from substrate scattering. The OTFT electrical characteristics were measured using a Keithley 4200-SCS in a N_2-filled glovebox. The μ_{FET} and threshold voltage (V_{Th}) values were calculated in the saturation region.

Fabrication of Thin-Film Transistors. The P3HT solution (1 wt % in toluene or *p*-xylene) was spin-coated on the glass or silicon wafer at a rotation speed of 1000 rpm in a N_2-filled glovebox. The film was then baked on a hot-plate at a temperature of 80 °C to remove residual solvent. The resultant thickness of the P3HT film was ~50 (in toluene) or ~30 nm (in *p*-xylene). To inscribe the order of the P3HT layers using CNT templates, P3HT-coated substrates (1.5 cm × 1.5 cm) were contacted with CNT templates under various loads (50, 100, 150, and 500 g, which are converted to ~2.2, 4.4, 6.5, and 22 kPa as a pressure unit) at 80 °C on a hot plate, and then the temperature was increased to 240 °C (above the melting temperature of P3HT). The thermal annealing was maintained for 30 min to obtain full contact between the P3HT layer and the CNTs, followed by slowly cooling to room temperature. The loaded CNT template was then removed from the P3HT film. For the polymer gate dielectric layers, poly(methyl methacrylate) (PMMA, molecular weight = 120 kD; Sigma–Aldrich) was used without further purification. PMMA (80 mg/mL) was dissolved in *n*-butyl acetate and the solution was filtered via a 0.45-μm polytetrafluoroethylene (PTFE) syringe filter before being spin-coated at 2000 rpm for 60 s. After dielectric coating to a thickness of 500–600 nm, the devices were finally annealed at 100 °C for 30 min in the same glovebox. Subsequently, top-gate and bottom-contact transistors were completed by forming gate electrodes on the active regions of the transistors by evaporation of aluminum layers (50–70 nm) with a metal shadow mask.

RESULTS AND DISCUSSION

To enable control of the orientation of the P3HT molecules by interactions with CNTs, the thermal properties such as melting and recrystallization temperature were analyzed using DSC under a N_2 atmosphere, as shown in the Supporting Information (Figure S1). P3HT melted and recrystallized at ca. 228 and 180 °C, respectively. Based on the thermal transition analysis result, we chose an annealing temperature of 240 °C, which is slightly higher than the melting temperature of P3HT, to obtain entirely new microstructures by template-assisted crystallization with VA-CNTs from the melting state. The melt solidification method for improving the crystallinity of a semiconducting layer in an OTFT has been reported.[10,34] However, the melt-solidified film exhibited random crystallite orientations of the conjugated polymers after cooling from the melting temperature. Thus, for the purpose of polymer chain alignment and orientation, "silicon based nanograting and nanoporous mold" or "anodic aluminum oxide (AAO) nanopore membranes" have been tried as templates by several research groups.[30,31] However, in those cases, the nanopore molds induced "random or isotropic P3HT chain orientation in the *x*–*y* plane" or "face-on crystallite formation" in the condition of SAM treated or bare mold.[30,31] To resolve this problem and induce the optimized polymer orientation for OTFTs, we used VA-CNT arrays ca. 300 nm in length and ca. 40 nm in diameter, embedded in AAO, for precise control of the orientation direction of the molecules in the melt-annealed films through π–π interaction between P3HT and CNTs. The SEM images in Figures 1a and 1b show the VA-CNT arrays, before the shallow molding process, with a uniformly exposed length of ~300 ± 50 nm and a diameter of ~40 nm ±10 on the AAO templates.

The schematic diagram in Figure 1c shows details of the experimental procedures. The spin-coated P3HT films were melt-annealed at 240 °C for 30 min without or with various pressures (2.2, 4.4, 6.5, and 22 kPa) produced by pressing with loads of 50, 100, 150, and 500 g in a N_2 atmosphere. The films were cooled naturally for more than 30 min without separation of the templates. Generally, for the nanoimprinting and

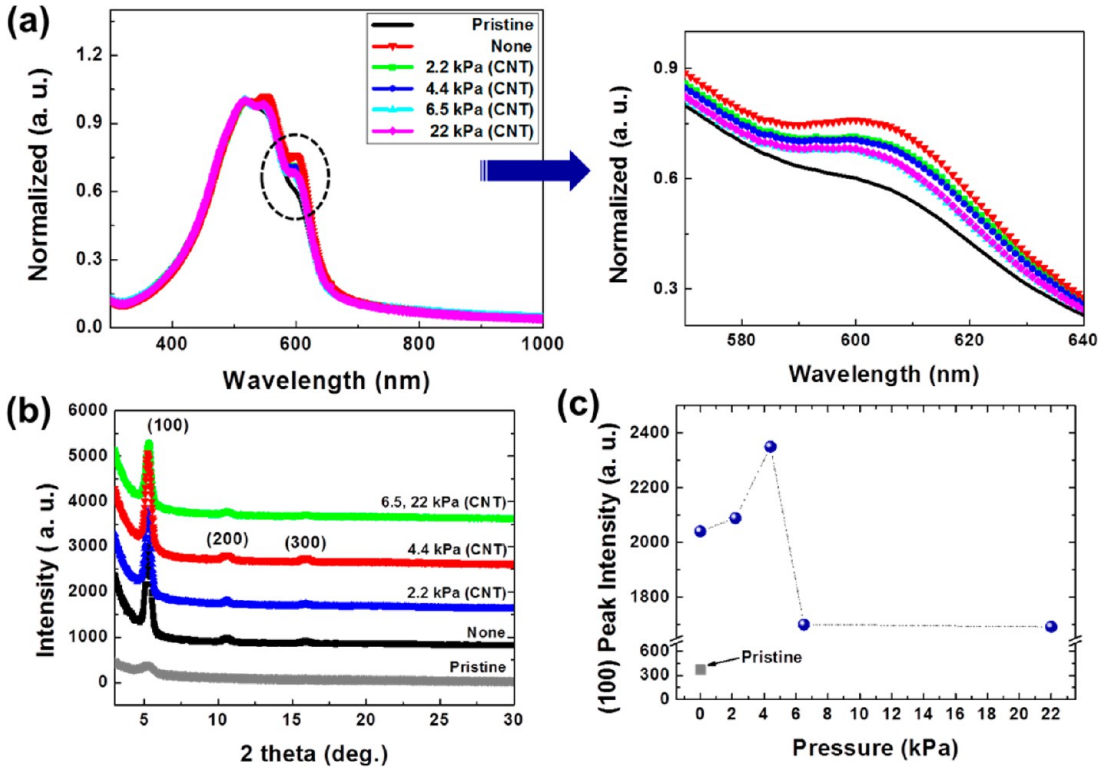

Figure 3. P3HT layer characteristic dependences upon annealing temperatures and pressures on VA-CNT arrays: (a) P3HT thin-film UV-vis absorption, (b) out-of plane XRD patterns, and (c) corresponding (100) peak intensities under various conditions: pristine (baking only), no VA-CNTs (only melt annealing), and pressed melt annealing with VA-CNT arrays under pressures of 2.2, 4.4, 6.5, and 22 kPa.

nanograting process of polymer film using silicone molds, the molds were treated with an antiadhesion monolayer (such as FDTS; 1H,1H,2H,2H-perfluorodecyltrichlorosilane).[31,32] The hydrophobic monolayer has a function to prevent the polymer from adhering to the nanostructure mold surface during its detachment step by reducing the mold surface energy.[32] However, VA-CNTs templates were used without a treatment of any other chemical monolayers in our experiments to investigate the effect of interaction between P3HT and CNTs. Because of the adhesion property between P3HT and CNTs, after the sequential process of separating the template from P3HT film at room temperature, some parts of the detached VA-CNT template from the P3HT film had P3HT residues attached on the surface, as shown in Figures 2a and 2b. These phenomena mean that the VA-CNTs template exfoliated the outermost surfaces of the P3HT layer in the detaching process between them, which will induce the rough surface layer. Meanwhile, the P3HT residues on the detached VA-CNTs array could indicate that the VA-CNTs were completely embedded in a few nanometers depth of the P3HT films by melting of the P3HT layer and pressing with loads. The surface morphologies of the P3HT film before and after melt-annealing with VA-CNTs were observed using AFM; the images are shown in Figures 2c and 2d, as well as in the Supporting Information (Figure S2). The surface morphologies of the P3HT films were changed by the melt-annealing process with the VA-CNTs template. The AFM images in Figure 2d and Figure S2b in the Supporting Information of a melt-annealed film under pressing with VA-CNTs show the presence of many trenches in the height range of 4−8 nm over the entire area of the film, unlike the melt-annealed sample without pressing with a VA-CNT template. In addition, the line root-mean-square roughness increased to 2.57 nm (with VA-CNTs) from 1.45 nm (none of VA-CNTs) in the line section of the AFM images in Figures 2c and 2d, as a result of the trenches produced by the VA-CNTs dissociating process from the melting annealed P3HT film at the end of template-assisted melt-annealing process.

To investigate the effect of VA-CNTs on the molecular orientations and crystallinities in P3HT films, various P3HT films, for the cases which were melt-annealed with VA-CNTs, melt-annealed without VA-CNTs, and baked at 80 °C, were characterized by UV-vis absorption spectra; the spectra are shown in Figure 3a. Three absorption peaks, at 520, 550, and 600 nm, were observed for all the samples. It is well-known that the first two peaks, at 520 and 550 nm, correspond to intrachain $\pi-\pi^*$ transitions, and the shoulder peak at 600 nm is related to interchain $\pi-\pi^*$ transitions.[13,35−37] All the melt-annealed films, with and without VA-CNTs, showed a larger absorption intensity at 600 nm, compared to the films baked at 80 °C, which were spin-coated from both toluene and *p*-xylene solutions (see Figure S3 in the Supporting Information). The pronounced absorption intensity at 600 nm of the melt-annealed films is attributed to strong intermolecular $\pi-\pi$ interactions as a result of improved crystallinities of the P3HT films.[36,37] The increased absorption intensities at 600 nm were maintained for the melt-annealed P3HT/VA-CNT films under various loads. These results mean that the average intermolecular packings and crystallinities in the melt-annealed P3HT films are very similar, with or without pressing with VA-CNTs templates.

For more precise information on the molecular orientation, we investigated the changes in the crystallinities and molecular orientations of the P3HT films using out-of plane XRD and

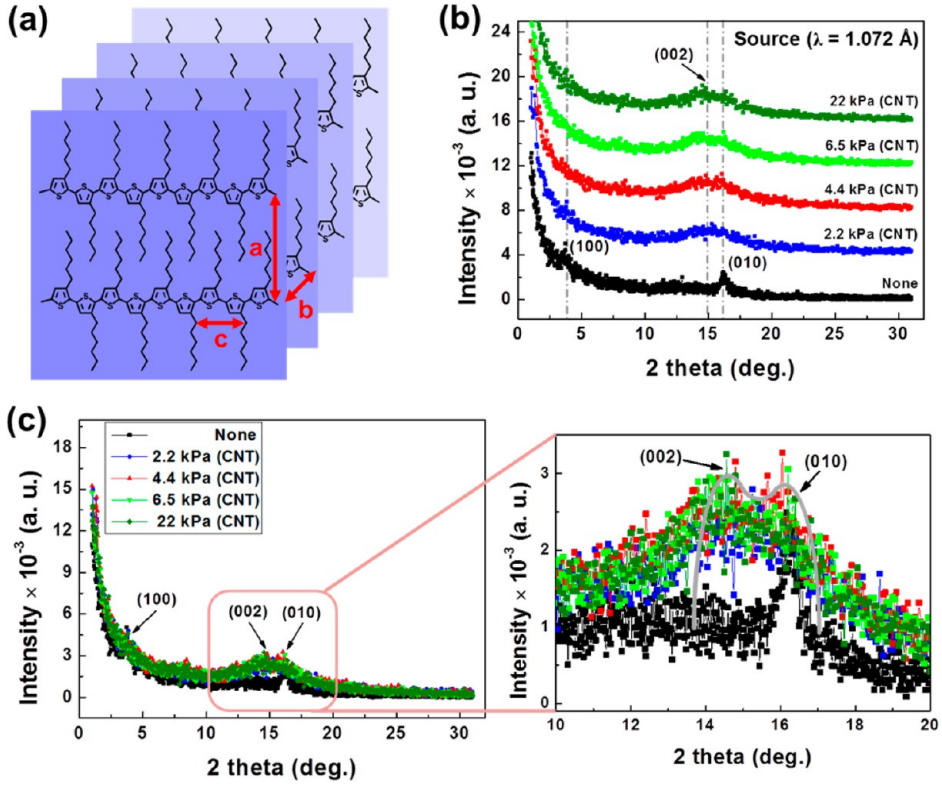

Figure 4. (a) Crystallite structure of P3HT with crystal axis units; (b) X-ray scattering patterns of P3HT thin films upon melt annealing without VA-CNT arrays and with VA-CNTs at pressures of 2.2, 4.4, 6.5, and 22 kPa, examined in grazing incidence in-plane mode; and (c) magnified view of in-plane XRD pattern in the diffraction angle range of 10°−20°.

GIXD measurements. A strong (100) reflection at 2θ = 5.26° and its corresponding weak higher-order peaks at θ = 10.52° (200) and 15.78° (300) were observed for all the melt-annealed films, with a lamellar repeating distance of 16.8 Å (see Figures 3b and 3c). The strong (h00) reflection peak in all of the out-of plane XRD data indicates that the P3HT $\pi-\pi$ stacking planes were oriented parallel to the substrate in the film (the so-called "edge-on orientation").[1,5,13] The intensity of the (100) peak increased gradually until the pressure load was 4.4 kPa, and then decreased sharply at a load of 6.5 kPa, as shown in Figures 3b and 3c. The increased (100) peaks with pressures of 2.2 and 4.4 kPa mainly should be the result of improved crystallite orientation in the P3HT film by interactions between P3HT and VA-CNTs, because the UV-vis absorption peak intensities at 600 nm are similar in the just-melt-annealed and VA-CNT melt-annealed P3HT films, which means that the films have similar crystallite densities.[36,37] The UV-vis absorption spectra and out-of plane XRD patterns show that a large number of P3HT chains are well-ordered in the lamellar structure, of which the $[h00]_{P3HT}$ direction is normal to the substrates, by melt annealing with VA-CNTs under a pressure of 2.2 or 4.4 kPa. The increase in the (100) peak in the melt-annealed P3HT film with VA-CNTs is caused not by an increased number of crystallites but by a higher fraction of the (h00) crystallite planes oriented to the normal direction of the substrate in the similar density of crystallites. In contrast, when the pressures on the VA-CNT array plates are increased to above 4.4 kPa, the diffraction intensities of the (100) plane normal to the substrates decreased significantly as a result of misoriented crystals nucleated probably from the inclined or bent VA-CNTs on the P3HT layers, caused by the bending strain of the CNTs or the AAO plate.

Although the UV-vis absorption spectra and out-of plane XRD patterns show that the melt-annealed P3HT film with a VA-CNT template has better crystallite orientation and packing properties, we must clarify the in-plane polymer chain ordering in the film since charge transport in OTFTs occurs in the direction parallel to the substrate through the transistor channel. It has been reported that polymer OTFTs exhibit the highest charge carrier mobility when the intrachain and interchain orientations are well-ordered within the polymer semiconductor crystallites, because the charge carriers can travel efficiently in two dimensions.[1,38,39] Therefore, GIXD was used to characterize the in-plane π-stacking of melt-annealed P3HT films using synchrotron X-ray radiation at the 10C1 Beamline Pohang Accelerator Laboratory. Figure 4 shows the in-plane XRD patterns of melt-annealed P3HT films without or with VA-CNT arrays under various loads. The GIXD data for the melt-annealed P3HT film without VA-CNTs arrays show (100) and (010) reflections coincidently, manifesting a $\pi-\pi$ stacking distance of 3.8 Å. These results imply that the simply melt-annealed film (none of VA-CNTs) contains P3HT crystallites in both face-on (those with the $\pi-\pi$ stacking direction lying out of the plane of the substrate) and edge-on (those with the $\pi-\pi$ stacking direction lying in the plane of the substrate) orientations. In particular, from the GIXD results for the melt-annealed P3HT films with VA-CNTs, the intensities of the (100) peaks were reduced compared with that of the just-melt-annealed film. Based on the in-plane and out-of-plane XRD results, a larger fraction of the (h00) axis of P3HT crystallites was oriented to the direction normal to the substrate in the P3HT/VA-CNTs films. In addition, a (002) peak was observed in the GIXD patterns of P3HT/VA-CNTs films, even although the (002) peak closely overlaps with the (010) peak

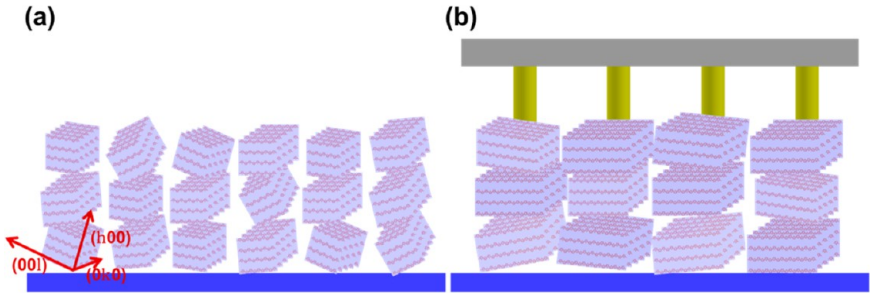

Figure 5. Schematic illustrations of (a) disordered P3HT (with no VA-CNT array), and (b) better-oriented P3HT crystallites in the in-plane and out-of plane directions obtained by melt annealing with a VA-CNT template.

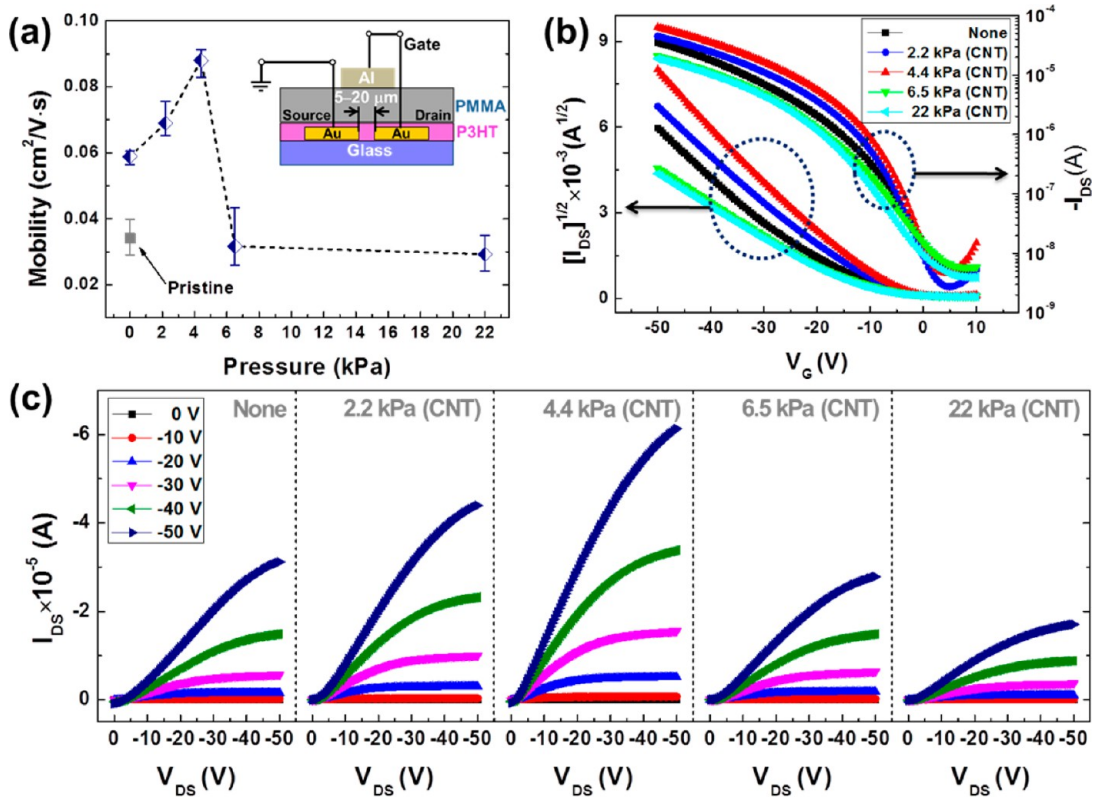

Figure 6. (a) Variations in charge carrier mobility in P3HT-based OTFTs (the inset shows a cross-section of P3HT top-gate and bottom-contact transistor); (b) corresponding transfer curves (at V_{DS} = −50 V); and (c) output curves in the cases of melt annealing without and with VA-CNTs under pressures of 2.2, 4.4, 6.5, and 22 kPa.

Table 1. Device Performances[a] of Melt-Annealed P3HT OTFTs under Various Pressures on VA-CNT Array Templates with Top-Gate and Bottom-Contact Device Geometry

process condition	mobility [$cm^2/(V\ s)$]	subthreshold swing, SS [V/dec]	on/off current ratio, I_{on}/I_{off}	threshold voltage, V_{th} [V]
pristine (no annealing)	0.029−0.039	6.6−9.5	2×10^3−5×10^3	−10.4 to −14.5
no CNT array	0.056−0.06	5.5−7.1	5×10^3− 9×10^3	0.4 to −13.4
VA-CNT array, under 2.2 kPa	0.065−0.075	4.2−5.6	9×10^3− 2×10^4	−3.4 to −13.0
VA-CNT array, under 4.4 kPa	0.083−0.12	4.2−4.9	2×10^3−1×10^4	0.4 to −6.5
VA-CNT array, under 6.5 kPa	0.026−0.043	5.6−8.9	2×10^3−9×10^3	−2.8 to −10.6
VA-CNT array, under 22 kPa	0.024−0.035	6.3−8.7	2×10^3−5×10^3	−1.7 to −10.9

[a]The field-effect mobility, SS, I_{on}/I_{off}, and V_{th} were calculated at the saturation region (V_{DS} = −50 V). The variation values of transistor performance under each process condition were calculated from the transfer curves measured in more than five distinct devices.

(see Figure 4c).[40−42] The presence of (002) peaks in the diffraction patterns of the P3HT/VA-CNTs films showed that the P3HT crystallites grew more extensively in the *c*-axis direction than the case of the merely melt-annealed P3HT film, in which only the (010) and (100) peaks were observed. The in-plane and out-of-plane XRD results indicate that wider P3HT nanoribbon crystallites are more aligned in the (*h*00) direction perpendicular to the substrate by melt annealing with VA-CNTs, as shown in the schematic diagram in Figure 5. The dominant charge transport route within the P3HT ordered

domains is along the intrachain direction instead of the interchain direction, because the charge transfer integral (i.e., the electron-coupling strength) along the interchain direction is significantly less than that along the intrachain direction.[38,43] Consequently, it is expected that the extended conjugation length in the nanoribbon crystallites, as a result of melt annealing of P3HT with VA-CNTs, could increase the charge carrier mobility of P3HT films in OTFTs.

For further observation of the relations between the P3HT ordering and orientations and their electrical properties for melt-annealed P3HT films with VA-CNTs, we used the melt-annealed P3HT films with VA-CNTs as active layers in top-gate, bottom-contact OTFT configurations, as depicted in the inset of Figure 6a. Figure 6 (along with Figure S5 in the Supporting Information) shows the field-effect mobilities of VA-CNTs-melt-annealed P3HT OFETs prepared from a 1 wt % solution in toluene (or *p*-xylene; see Figure S5 in the Supporting Information). In addition, the device performances at the various process conditions are summarized in Table 1, which reveals mobility, subthreshold swing (SS), on/off current ratio (I_{on}/I_{off}), and threshold voltage (V_{th}). As observed in UV-vis spectroscopy, the just-melt-annealed P3HT revealed better charge mobility (0.056−0.06 $cm^2/(V\ s)$) than the pristine case (0.029−0.039 $cm^2/(V\ s)$), because of its increased crystallinity. As well, the transistor of P3HT film annealed in melting state with a VA-CNT template under a pressure of 4.4 kPa showed a field-effect mobility up to 0.12 $cm^2/(V\ s)$, which was improved two times compared to the merely melt-annealed device without VA-CNTs. Overall, the general trend in the field-effect mobility is consistent with the measured crystallite-orientation trends of the melt-annealed P3HT films observed by out-of plane and in-plane XRD analysis. However, the degree of increase is somewhat lower than we expected. The relatively modest enhancement of the field-effect mobility mainly would be a result of the large P3HT surface roughness, which was caused by the slightly embedded VA-CNT array in the P3HT film during the melt annealing and subsequent detaching process (see Figures 2c and 2d). Although better ordering and orientation of the P3HT molecules and larger crystal domains were obtained by melt annealing with VA-CNTs, the large surface roughness and deep valleys (up to ∼10 nm) at the semiconductor/dielectric interface could scatter charge carriers and interrupt charge carrier transport in P3HT OTFTs with top-gate configuration.[36,44]

CONCLUSION

In this paper, we report a method for controlling the molecular orientations of conjugated polymers in thin films by melt annealing with the simple pressing of vertically aligned multiwall carbon nanotube (VA-CNT) arrays. The melt-annealed P3HT films with VA-CNTs exhibited the improved crystallite ordering and orientation compared to the melt-annealed films without the arrays, despite a similar density of crystallites with a merely melt-annealed film. In addition, most of the crystallites of the P3HT films were oriented preferentially in the [100] direction, normal to the substrates after the melt annealing with VA-CNTs. Moreover, the crystallite has been extended longer in the direction of conjugation axis (*c*-axis; [001]) peculiarly. Consequently, the melt-annealing-assisted P3HT films with VA-CNTs were used as active layer in organic thin-film transistors (OTFTs), and the P3HT field-effect transistors exhibited a higher charge carrier mobility—up to 0.12 $cm^2/(V\ s)$—than merely melt-annealed P3HT devices. After all, the nucleation growth and reordering of polymer crystallites from VA-CNTs template would be a very useful and potential process for the improvement of charge transport in organic electronics.

ASSOCIATED CONTENT

Supporting Information

(1) DSC curve for P3HT thermal behavior, and AFM topographical images (1 μm × 1 μm) of the P3HT thin films. (2) Table and figure of device characteristics, UV−vis absorption spectra and out-of plane X-ray diffraction patterns of P3HT films prepared from *p*-xylene. (3) The electrical characteristics of bottom-gate and top-contact P3HT transistor. This material is available free of charge via the Internet at http://pubs.acs.org.

AUTHOR INFORMATION

Corresponding Author

*E-mail addresses: kimdy@gist.ac.kr (D.-Y.K.), yynoh@dongguk.edu (Y.-Y.N.).

Notes

The authors declare no competing financial interest.

ACKNOWLEDGMENTS

This work was supported by the National Research Foundation of Korea (NRF) grant funded by the Korea government (MSIP) (No. 2012-0008723) and by a grant from the Center for Advanced Soft Electronics (No. 2012054547), under the Global Frontier Research Program of the MEST. This work also was supported by the Dongguk University Research Fund of 2013.

ABBREVIATIONS

AAO = anodic aluminum oxide
AFM = atomic force microscopy
CNTs = carbon nanotubes
DSC = differential scanning calorimetry
μ_{FET} = field-effect mobility
GXID = grazing-incidence XRD
MWCNT = multiwalled carbon nanotube
NIR = near-infrared
OTFTs = organic thin-film transistors
OTS = octadecyltrichlorosilane
P3HT = poly(3-hexylthiophene)
PAL = Pohang Accelerator Laboratory
PMMA = poly(methyl methacrylate)
rr-P3HT = regioregular poly(3-hexylthiophene)
SAM = self-assembled monolayer
SEM = scanning electron microscopy
UV = ultraviolet
VA-CNTs = vertically aligned multiwalled carbon nanotubes
vis = visible
XRD = X-ray diffraction

REFERENCES

(1) Sirringhaus, H.; Brown, P. J.; Friend, R. H.; Nielsen, M. M.; Bechgaard, K.; Langeveld-Voss, B. M. W.; Spiering, A. J. H.; Janssen, R. A. J.; Meijer, E. W.; Herwig, P.; de Leeuw, D. M. *Nature* **1999**, *401*, 685−688.

(2) Yan, H.; Chen, Z.; Zheng, Y.; Newman, C.; Quinn, J. R.; Dötz, F.; Kastler, M.; Facchetti, A. *Nature* **2009**, *457*, 679−686.

(3) Caironi, M.; Bird, M.; Fazzi, D.; Chen, Z.; Pietro, R. D.; Newman, C.; Facchetti, A.; Sirringhaus, H. *Adv. Funct. Mater.* **2011**, *21*, 3371−3381.
(4) Rivnay, J.; Mannsfeld, S. C. B.; Miller, C. E.; Salleo, A.; Toney, M. F. *Chem. Rev.* **2012**, *112*, 5488−5519.
(5) Kline, R. J.; McGehee, M. D.; Toney, M. F. *Nat. Mater.* **2006**, *5*, 222−228.
(6) Chabinyc, M. L.; Toney, M. F.; Kline, R. J.; McCulloch, I.; Heeney, M. *J. Am. Chem. Soc.* **2007**, *129*, 3226−3237.
(7) Friend, R. H.; Gymer, R. W.; Holmes, A. B.; Burroughes, J. H.; Marks, R. N.; Taliani, C.; Bradley, D. D. C.; Dos Santos, D. A.; Brédas, J. L.; Lögdlund, M.; Salaneck, W. R. *Nature* **1999**, *397*, 121−128.
(8) Burroughes, J. H.; Bradley, D. D. C.; Brown, A. R.; Marks, R. N.; Mackay, K.; Friend, R. H.; Burns, P. L.; Holmes, A. B. *Nature* **1990**, *347*, 539−541.
(9) Kim, Y.; Cook, S.; Tuladhar, S. M.; Choulis, S. A.; Nelson, J.; Durrant, J. R.; Bradley, D. D. C.; Giles, M.; McCulloch, I.; Ha, C.-S.; Ree, M. *Nat. Mater.* **2006**, *5*, 197−203.
(10) Rivnay, J.; Steyrleuthner, R.; Jimison, L. H.; Casadei, A.; Chen, Z.; Toney, M. F.; Facchetti, A.; Neher, D.; Salleo, A. *Macromolecules* **2011**, *44*, 5246−5255.
(11) Sirringhaus, H.; Tessler, N.; Friend, R. H. *Science* **1998**, *280*, 1741−1744.
(12) Ong, B. S.; Wu, Y.; Liu, P.; Gardner, S. *J. Am. Chem. Soc.* **2004**, *126*, 3378−3379.
(13) Kim, D. H.; Park, Y. D.; Jang, Y.; Yang, H.; Kim, Y. H.; Han, J. I.; Moon, D. G.; Park, S.; Chang, T.; Chang, C.; Joo, M.; Ryu, C. Y.; Cho, K. *Adv. Funct. Mater.* **2005**, *15*, 77−82.
(14) Bao, Z.; Dodabalapur, A.; Lovinger, A. J. *Appl. Phys. Lett.* **1996**, *69*, 4108−4110.
(15) Kline, R. J.; McGehee, M. D.; Kadnikova, E. N.; Liu, J.; Fréchet, J. M. J. *Adv. Mater.* **2003**, *15*, 1519−1522.
(16) Chang, J.-F.; Sun, B.; Breiby, D. W.; Nielsen, M. M.; Sölling, T. I.; Giles, M.; McCulloch, I.; Sirringhaus, H. *Chem. Mater.* **2004**, *16*, 4772−4776.
(17) Yang, H.; Shin, T. J.; Yang, L.; Cho, K.; Ryu, C. Y.; Bao, Z. *Adv. Funct. Mater.* **2005**, *15*, 671−676.
(18) Veres, J.; Ogier, S.; Lloyd, G.; de Leeuw, D. *Chem. Mater.* **2004**, *16*, 4543−4555.
(19) Chua, L.-L.; Zaumseil, J.; Chang, J.-F.; Ou, E. C.-W.; Ho, P. K.-H.; Sirringhaus, H.; Friend, R. H. *Nature* **2005**, *434*, 194−199.
(20) Ito, Y.; Virkar, A. A.; Mannsfeld, S.; Oh, J. H.; Toney, M.; Locklin, J.; Bao, Z. *J. Am. Chem. Soc.* **2009**, *131*, 9396−9404.
(21) Sirringhaus, H. *Adv. Mater.* **2005**, *17*, 2411−2425.
(22) Saini, V.; Li, Z.; Bourdo, S.; Dervishi, E.; Xu, Y.; Ma, X.; Kunets, V. P.; Salamo, G. J.; Viswanathan, T.; Biris, A. R.; Saini, D.; Biris, A. S. *J. Phys. Chem. C* **2009**, *113*, 8023−8029.
(23) Kang, Y. K.; Lee, O.-S.; Deria, P.; Kim, S. H.; Park, T.-H.; Bonnell, D. A.; Saven, J. G.; Therien, M. J. *Nano Lett.* **2009**, *9*, 1414−1418.
(24) Cheng, F.; Imin, P.; Maunders, C.; Botton, G.; Adronov, A. *Macromolecules* **2008**, *41*, 2304−2308.
(25) Li, L.; Li, C. Y.; Ni, C. *J. Am. Chem. Soc.* **2006**, *128*, 1692−1699.
(26) Liu, J.; Zou, J.; Zhai, L. *Macromol. Rapid Commun.* **2009**, *30*, 1387−1391.
(27) Zou, J.; Khondaker, S. I.; Huo, Q.; Zhai, L. *Adv. Funct. Mater.* **2009**, *19*, 479−483.
(28) Kim, D. H.; Shin, H.-J.; Lee, H. S.; Lee, J.; Lee, B.-L.; Lee, W. H.; Lee, J.-H.; Cho, K.; Kim, W.-J.; Lee, S. Y.; Choi, J.-Y.; Kim, J. M. *ACS Nano* **2012**, *6*, 662−670.
(29) Sun, Z.; Li, J.; Liu, C.; Yang, S.; Yan, F. *Adv. Mater.* **2011**, *23*, 3648−3652.
(30) Kim, J. S.; Park, Y.; Lee, D. Y.; Lee, J. H.; Park, J. H.; Kim, J. K.; Cho, K. *Adv. Funct. Mater.* **2010**, *20*, 540−545.
(31) Aryal, M.; Trivedi, K.; Hu, W. *ACS Nano* **2009**, *3*, 3085−3090.
(32) Kim, Y.-S.; Lee, K.; Lee, J. S.; Jung, G. Y.; Kim, W. B. *Nanotechnology* **2008**, *19*, 365305.
(33) Kim, Y.-S.; Ahn, H.-J.; Nam, S. H.; Lee, S. H.; Shim, H.-S.; Kim, W. B. *Appl. Phys. Lett.* **2008**, *93*, 103104.
(34) Tsao, H. N.; Cho, D. M.; Park, I.; Hansen, M. R.; Mavrinskiy, A.; Yoon, D. Y.; Graf, R.; Pisula, W.; Spiess, H. W.; Müllen, K. *J. Am. Chem. Soc.* **2011**, *133*, 2605−2612.
(35) Brown, P. J.; Sirringhaus, H.; Harrison, M.; Shkunov, M.; Friend, R. H. *Phys. Rev. B* **2001**, *63*, 125204.
(36) Zhao, K.; Ding, Z.; Xue, L.; Han, Y. *Macromol. Rapid Commun.* **2010**, *31*, 532−538.
(37) Zhang, Y.; Tajima, K.; Hashimoto, K. *Macromolecules* **2009**, *42*, 7008−7015.
(38) Lan, Y.-K.; Huang, C.-I *J. Phys. Chem. B* **2008**, *112*, 14857−14862.
(39) Crossland, E. J. W.; Tremel, K.; Fischer, F.; Rahimi, K.; Reiter, G.; Steiner, U.; Ludwigs, S. *Adv. Mater.* **2012**, *24*, 839−844.
(40) Prosa, T. J.; Winokur, M. J.; Moulton, J.; Smith, P.; Heeger, A. J. *Macromolecules* **1992**, *25*, 4364−4372.
(41) Jimison, L. H.; Toney, M. F.; McCulloch, I.; Heeny, M.; Salleo, A. *Adv. Mater.* **2009**, *21*, 1568−1572.
(42) Colle, R.; Grosso, G.; Ronzani, A.; Zicovich-Wilson, C. M. *Phys. Status Solidi B* **2011**, *248*, 1360−1368.
(43) Lan, Y.-K.; Huang, C.-I *J. Phys. Chem. B* **2009**, *113*, 14555−14564.
(44) Chua, L.-L.; Ho, P. K. H.; Sirringhaus, H.; Friend, R. H. *Adv. Mater.* **2004**, *16*, 1609−1615.